

Cluster theory of Janus particles

Riccardo Fantoni*

*National Institute for Theoretical Physics (NITheP) and Institute of Theoretical Physics,
Stellenbosch University, Stellenbosch 7600, South Africa*

Achille Giacometti†

Dipartimento di Chimica Fisica, Università di Venezia, S. Marta DD2137, I-30123 Venezia, Italy

Francesco Sciortino‡

Dipartimento di Fisica, Università di Roma La Sapienza, Piazzale A. Moro 2, 00185 Roma, Italy

Giorgio Pastore§

Dipartimento di Fisica dell' Università, Strada Costiera 11, 34151 Trieste, Italy

(Dated: May 26, 2022)

We apply a simple statistical mechanics cluster approximation for studying clustering in the Kern and Frenkel model of Janus fluids. The approach is motivated by recent Monte Carlo simulations work on the same model revealing that the vapor coexisting with the liquid phase contains clusters of different sizes and shapes whose equilibrium concentrations in general depend on the interaction range as well as on thermodynamic parameters. The approximation hinges on a separation between the intra- and inter-cluster contribution to thermodynamics, where only the former is explicitly computed by Monte Carlo simulations. Two levels of a simple liquid theory approximation are exploited for the description of the latter. In the first we use the ideal-gas expressions and obtain a qualitative agreement with extensive Monte Carlo bulk simulations. This can be improved to a semi-quantitative agreement, by using a hard-sphere description for the cluster-cluster correlations.

PACS numbers: 64.60.-i, 64.70.-p, 64.70.Fx, 64.60.Ak

Keywords: Janus particles, Kern-Frenkel model, cluster theory, Monte Carlo simulation

I. INTRODUCTION

Recent advances in experimental techniques for chemical synthesis have provided a well defined set of different protocols for obtaining colloidal particles with different shapes, chemical compositions and surface patterns. In particular it is now possible to obtain colloidal particles with pre-defined number and distribution of solvophobic and solvophilic regions on their surface. These are usually referred to as patchy colloids.¹⁻⁴

The simplest example within this realm is constituted by the so-called Janus particles, where the surface is partitioned in only two parts with even distribution of the two philicities. In spite of their apparent simplicity, Janus particles have aroused increasingly interest in the last few years both for their potential technological applications and in view of the rather unusual displayed self-assembly properties as compared to conventional isotropic colloidal particles.⁵⁻⁸

A detailed study of the fluid-fluid transition for Janus fluids has recently been carried out by Monte Carlo (MC) simulation^{9,10} using the Kern-Frenkel pair potential¹¹. Within this model, the solvophobic and solvophilic hemispheres are mimicked by an attractive square-well potential and a repulsive hard-sphere potential respectively, and two spheres attract each other only provided that their centers are within a given distance, as dictated by the width of the well, and the two attractive patches on each sphere are properly aligned one another, that is lie within a predefined relative angular range.

The combined features of the equal amplitude of the two philicities coupled with the specificity of the chosen potential types, give rise to a micellization process originating in the vapor phase that severely destabilizes the condensation process thus providing a re-entrant vapour coexistence curve that in the temperature-density diagram is skewed toward higher densities as the system is cooled to lower temperatures⁹. A number of additional unusual features were also found for the vapour phase¹⁰, including the fact that, for the chosen width of the square-well potential (50% of the particle size), there appeared a predominance of particular clusters formed by single-layer (micelles of about 10 particle) and double-layer (vesicles of about 40 particles) always exposing the hard-sphere part as an external global surface, thus inhibiting the formation of a liquid phase.

It should be emphasized that MC simulations are particularly demanding for this system in such that very low temperatures (of the order of 0.25 or less in reduced units) are necessary to observe these phenomena, and this is expected to be even more demanding for decreasing range of the interactions¹⁰.

In this paper, we focus our interest to the study of the vapor phase, following a different approach, hinging on a strategy similar to that devised in the context of associating fluids, where several different theories with different

degrees of success have been envisioned.^{12–15}

Our approach has been inspired by the work of Tani and Henderson¹⁶, extending the Bjerrum theory for association in electrolytic solutions¹⁷ where the total partition function is factorized into a intra- and inter-cluster contribution, so that the original task is reduced to the computation of the partition function for clusters of increasing sizes along with the interaction among them.

While the original approach¹⁶ was limited by the necessity of evaluating analytically even the intra-cluster partition function, in addition to the inter-cluster contribution, we propose to determine the former by explicit Monte Carlo simulations for each cluster and the latter using physically motivated fluid theories. Within MC simulation of each n -cluster, we are then able to determine the energy per particle as a function of temperature and thereby compute the excess free energy of the isolated cluster by thermodynamic integration.

Clearly, this approach is particularly suited to study the vapor phase as once the first n -particle clusters have been simulated the resulting information can be inserted in the inter-cluster theory, and this is enough to determine the partition function of the vapor at all thermodynamic states. We can then follow and predict the dependence of cluster population on thermodynamic conditions and interaction parameters. This is particularly relevant in cases in which spontaneous cluster formation is particularly slow, due for example to the low value of the temperature at which clustering takes place, a common case when the interaction range is very short.

The paper is organized as follows: in section II we describe the model, in sections III and IV we introduce the cluster theory, in section V we describe how we determined the intra-cluster partition function. Additional results are then presented in section VI, and section VII is for final remarks.

II. THE KERN AND FRENKEL MODEL

As in the work of Sciortino *et. al.*^{9,10} we used the Kern and Frenkel¹¹ patchy hard sphere model to describe the Janus fluid. Two spherical particles attract via a short-range square-well potential only if the line segment joining the centers of the two spheres intercepts a patch on the surface of the first particle and one on the surface of the other. In the case of a *single* patch per particle, the pair potential reads¹¹

$$\Phi(1, 2) = \phi(r_{12})\Psi(\hat{\mathbf{n}}_1, \hat{\mathbf{n}}_2, \hat{\mathbf{r}}_{12}), \quad (2.1)$$

where

$$\phi(r) = \begin{cases} +\infty & r < \sigma \\ -\epsilon & \sigma < r < \lambda\sigma \\ 0 & \lambda\sigma < r \end{cases} \quad (2.2)$$

and

$$\Psi(\hat{\mathbf{n}}_1, \hat{\mathbf{n}}_2, \hat{\mathbf{r}}_{12}) = \begin{cases} 1 & \text{if } \hat{\mathbf{n}}_1 \cdot \hat{\mathbf{r}}_{12} \geq \cos \theta_0 \text{ and } -\hat{\mathbf{n}}_2 \cdot \hat{\mathbf{r}}_{12} \geq \cos \theta_0 \\ 0 & \text{otherwise} \end{cases} \quad (2.3)$$

where θ_0 is the angular semi-amplitude of the patch. Here $\hat{\mathbf{n}}_1(\omega_1)$ and $\hat{\mathbf{n}}_2(\omega_2)$ are unit vectors giving the directions of the center of the patch in spheres 1 and 2, respectively, with $\omega_1 = (\theta_1, \varphi_1)$ and $\omega_2 = (\theta_2, \varphi_2)$ their corresponding spherical angles in an arbitrary oriented coordinate frame. Similarly, $\hat{\mathbf{r}}_{12}(\Omega)$ is the unit vector of the separation r_{12} between the centers of the two spheres and is defined by the spherical angle Ω . As usual, we have denoted with σ the hard core diameter and $\lambda = 1 + \Delta/\sigma$ with Δ the width of the well.

One can define the fraction of surface covered by the attractive patch as

$$\chi = \langle \Psi(\hat{\mathbf{n}}_1, \hat{\mathbf{n}}_2, \hat{\mathbf{r}}_{12}) \rangle_{\omega_1, \omega_2}^{1/2} = \sin^2 \left(\frac{\theta_0}{2} \right). \quad (2.4)$$

where we have introduced $\langle \dots \rangle_{\omega} = (1/4\pi) \int d\omega(\dots)$ as the average over the solid angle ω .

Reduced units $k_B T/\epsilon$ (k_B is the Boltzmann constant) and $\rho\sigma^3$ will be used as a measure of the temperature and density in numerical data.

III. A CLUSTER THEORY FOR JANUS PARTICLES

Following Ref. 16, we split the partition function in an inter- and intra-cluster contribution. Let N_n be the number of clusters formed by n particles, where $n = 1, \dots, n_c$ (n_c being the number of different clusters) and $\rho_n = N_n/V$

their density. We then write the total partition function as

$$Q_{\text{tot}} = \sum'_{\{N_n\}} \left[\prod_{n=1}^{n_c} \frac{1}{N_n!} (q_n^{\text{intra}})^{N_n} \right] Q_{\text{inter}}(\{N_n\}, V, T) , \quad (3.1)$$

where the prime indicates that the sum is restricted to all possible configurations satisfying the obvious constraint of conserving the total number of particles N ,

$$\sum_{n=1}^{n_c} nN_n = N . \quad (3.2)$$

Here q_n^{intra} is the “internal” partition function for a n -particle cluster and $Q_{\text{inter}}(\{N_n\}, V, T)$ is the inter-cluster partition function. Additional controlled thermodynamic variables are the total volume V and the temperature T .

The constraint can be dealt with by introducing a Lagrange multiplier so that we minimize the quantity

$$\ln \hat{Q}_{\text{tot}} = \ln Q_{\text{tot}} + (\ln \lambda) \sum_{n=1}^{n_c} nN_n . \quad (3.3)$$

In computing the partition function (3.1) we assume that the sum can be replaced by its largest dominant contribution. With the help of Stirling approximation $N! \approx (N/e)^N$ one then obtains

$$\ln Q_{\text{tot}} \approx \sum_{n=1}^{n_c} [N_n \ln q_n^{\text{intra}} - (N_n \ln N_n - N_n)] + \ln Q_{\text{inter}} . \quad (3.4)$$

The correct cluster distribution $\{\bar{N}_n\}$ is then found from the variational condition

$$\left. \frac{\partial}{\partial N_n} \ln \hat{Q}_{\text{tot}} \right|_{\{N_n = \bar{N}_n\}} = 0 . \quad (3.5)$$

This allows the calculation of the resulting free energy, $\beta F_{\text{tot}} = -\ln Q_{\text{tot}}$, in terms of the internal reduced free energy densities, $\beta f_n^{\text{intra}} = -\ln q_n^{\text{intra}}$, so that

$$\frac{\beta F_{\text{tot}}}{V} = \sum_{n=1}^{n_c} [\bar{\rho}_n \ln \bar{\rho}_n - \bar{\rho}_n] + \sum_{n=1}^{n_c} \bar{\rho}_n \beta f_n^{\text{intra}} + \sum_{n=1}^{n_c} \bar{\rho}_n \ln V - \frac{1}{V} \ln Q_{\text{inter}} . \quad (3.6)$$

In the above expression, $\beta = 1/(k_B T)$.

IV. SPECIFIC MODELS

We now consider two specific cases, where the inter-cluster interaction is not accounted for (the ideal-gas case) or modeled as an effective hard-sphere like interaction between clusters.

A. Ideal gas

The simplest possibility corresponds to consider different clusters as non-interacting ideal particles so that

$$Q_{\text{inter}}(\{N_n\}, V, T) = \prod_{n=1}^{n_c} \left(\frac{V}{\Lambda_n^3} \right)^{N_n} \equiv Q_{\text{ideal}} , \quad (4.1)$$

where Λ_n is the de Broglie thermal wavelength associated with each n -cluster.

Using Eqns. (3.5) and (4.1) one easily obtains

$$\bar{\rho}_n = \lambda^n \frac{q_n^{\text{intra}}}{\Lambda_n^3} , \quad (4.2)$$

where $\bar{\rho}_n = \bar{N}_n/V$.

The actual value of the Lagrange multiplier λ can then be numerically obtained upon inverting the constraint (3.2)

$$\sum_{n=1}^{n_c} n \lambda^n \frac{q_n^{\text{intra}}}{\Lambda_n^3} = \rho \equiv \frac{N}{V}. \quad (4.3)$$

Substitution of Eq. (4.1) into the general expression of the free energy (3.6) leads to¹⁸

$$\frac{\beta F_{\text{tot}}}{V} = \sum_{n=1}^N [\bar{\rho}_n \ln(\bar{\rho}_n \Lambda_n^3) - \bar{\rho}_n] + \sum_{n=1}^N \bar{\rho}_n \beta f_n^{\text{intra}}. \quad (4.4)$$

B. Chemical equilibrium

The above result (4.4) can be used to compute chemical equilibrium among different clusters. Indeed, on defining μ_n as the chemical potential associated to the n -th cluster, we have

$$\beta \mu_n = \frac{\partial(\beta F_{\text{tot}})}{\partial N_n} = \frac{\partial(\beta F_{\text{tot}}/V)}{\partial \rho_n} = \ln(\rho_n \Lambda_n^3) + \beta f_n^{\text{intra}} \quad (4.5)$$

We can then impose the equilibrium condition $\mu_n = n\mu_1$ to obtain

$$f_n^{\text{intra}} = n f_1^{\text{intra}} + k_B T \ln \left[\frac{\rho_n \Lambda_n^3}{(\rho_1 \Lambda_1^3)^n} \right] \quad (4.6)$$

which can be used to compute the internal free energies, given the cluster distributions. An alternative procedure, based on the explicit computation of the internal energy per particle within each cluster, will be discussed in Section IV.

C. Connection with Wertheim association theory

An interesting comparison can be found with Wertheim first-order association theory¹² which is frequently used in this context (see e.g. Ref.19 and references therein). Within this theory, the bond contribution to the Hemholtz free energy can be computed from a chemical equilibrium equation under the condition that only a suitable subset of diagrams are included in the cluster expansion and each attractive site is engaged at most in a single bond, the limit of a single-bond per patch in the language of the present paper.

Consider a system formed by only monomers and dimers, that is $n = 1, 2$. Then from Eq.(4.2) and condition (3.2) limited to $n = 1, 2$ we can obtain a quadratic equation in the Lagrange multiplier λ . The only acceptable root can then be substituted into Eq.(4.2) for $n = 1$ to obtain the fraction of patches that are not bonded, that is the fraction of monomers

$$\frac{\bar{\rho}_1}{\rho} = \frac{2}{1 + \sqrt{1 + 8\rho\bar{\Delta}}}, \quad (4.7)$$

Using numerical simulations for $n = 1, 2$ clusters we are able to determine the energy per particle in an n -cluster as a function of temperature and thereby determine the excess free energy of the isolated cluster by integration where $\bar{\Delta} = (q_2^{\text{intra}}/[q_1^{\text{intra}}]^2)(\Lambda_1^2/\Lambda_2)^3$. This equation is identical to the result from Wertheim's theory (see Eq.(10) in Ref.19) when translated in the appropriate language. Therefore, the present formulation is equivalent to Wertheim's theory provided that temperatures are sufficiently low (see Ref. 19 for further details) and the condition single-bond per binding site is satisfied. On the other hand, the present theory allows for an arbitrary amplitude of the patch thus including the possibility of multiple bonding.

Note that while in the case of only two clusters ($n = 1, 2$) requires the solution of a system of 2 coupled equations that results into a quadratic equation for λ , a general case with clusters up to the total number of clusters n_c clearly requires the solution of a system of n_c coupled equation, a task that – in general – has to be carried out numerically.

D. Effective hard sphere inter-cluster interaction

While simple, the ideal gas is clearly rather unphysical even at very low densities. A more physical description amounts to consider all n -particle clusters as identical hard spheres with diameters σ_n and packing fractions $\eta_n = (\pi/6)\rho_n\sigma_n^3$. A rather precise approximate solution in this case is provided by the Boublík, Mansoori, Carnahan, and Starling expression^{20,21}, but for simplicity we here only consider the case $\sigma_n = \sigma_0$ for all n , whose thermodynamics is well described by the simple monodisperse Carnahan-Starling formulae²². This can be motivated by the fact that only a minor variation is found in the linear cluster dimensions (see Table I and discussion further below) and by the observation that instantaneous size variations of an n -particle cluster are comparable with the variation of the average cluster radii for n within a few tens. It is then attempting to approximate the correlations between different shaped populations of clusters by a single effective one-component hard sphere system to take care of the average inter-cluster correlations.

Then

$$Q_{\text{inter}}(\{N_n\}, V, T) = Q_{\text{ideal}} e^{-\beta F_{\text{cs}}} , \quad (4.8)$$

where Q_{ideal} is given in Eq. (4.1) and F_{cs} is the Carnahan-Starling²³ excess free energy

$$\frac{\beta F_{\text{cs}}(\eta_t)}{N_t} = \frac{\eta_t(4 - 3\eta_t)}{(1 - \eta_t)^2} , \quad (4.9)$$

where $N_t = \sum_{n=1}^{n_c} N_n$ is the total number of clusters and $\eta_t = \sum_{n=1}^{n_c} \eta_n$ is the total cluster packing fraction. Following the same steps as before one obtains

$$\bar{\rho}_n = \lambda^n \frac{q_n^{\text{intra}}}{\Lambda_n^3} G(\eta_t) , \quad (4.10)$$

where we have introduced the function

$$G(x) = \exp \left[-\frac{x(8 - 9x + 3x^2)}{(1 - x)^3} \right] . \quad (4.11)$$

For the free energy one obtains from Eq. (3.6)

$$\frac{\beta F_{\text{tot}}}{V} = \sum_{n=1}^{n_c} [\bar{\rho}_n \ln(\bar{\rho}_n \Lambda_n^3) - \bar{\rho}_n] + \sum_{n=1}^{n_c} \bar{\rho}_n \beta f_n^{\text{intra}} + \frac{\beta F_{\text{cs}}(\bar{\eta}_t)}{V} , \quad (4.12)$$

that differs from the ideal gas counterpart Eq. (4.4) only for the last additional term. Clearly one recovers the ideal gas in the limit $\bar{\rho}_n \rightarrow 0$ as it should. In order to find the correct solution for this system of equation it is important to choose the one that is continuously obtained from the solution of the ideal gas case at $\sigma_0 \rightarrow 0$.

E. Thermodynamic quantities

It proves convenient to express our analysis in terms of reduced partition functions Z rather than of the full partition functions Q used in Section III. This can be conveniently done by the definitions

$$Q_{\text{inter}} = \prod_{n=1}^{n_c} \frac{Z_{\text{inter}}}{\Lambda_n^{3N_n}} \quad q_n^{\text{intra}} = \Lambda_n^3 Z_n^{\text{intra}} . \quad (4.13)$$

Given the partition function Q_{tot} we can determine the Carnahan-Starling excess free energy

$$\beta F^{\text{exc}} = -\ln \left(\frac{Q_{\text{tot}}}{V^N} \right) , \quad (4.14)$$

the internal energy per particle

$$u = \frac{3}{2\beta} + \frac{1}{N} \frac{\partial(\beta F^{exc})}{\partial\beta} = \frac{3}{2\beta} - \sum_{n=1}^{n_c} \frac{N_n}{N} \frac{\partial(\ln Z_n^{intra})}{\partial\beta} = \frac{3}{2\beta} + \sum_{n=1}^{n_c} n \frac{N_n}{N} u_n(T), \quad (4.15)$$

where u_n is the internal energy per particle of an n -cluster (see Section IV). We can also determine the compressibility factor

$$\frac{\beta P}{\rho} = \frac{1}{\rho} \frac{\partial(\ln Q_{tot})}{\partial V} = \frac{1}{\rho} \frac{\partial(\ln Z_{inter})}{\partial V} = \frac{1 + \eta_t + \eta_t^2 - \eta_t^3}{(1 - \eta_t)^3}. \quad (4.16)$$

V. COMPUTATION OF THE INTRA-CLUSTER FREE ENERGY

The simulation were carried out following the same prescription used for the bulk fluid phases^{9,10}. Two kind of moves for each chosen particle – a random translation and a random rotation – were allowed, following standard recipes²⁴ and a standard Metropolis²⁵ algorithm was used to compute the energy per particle of the system of n particles.

Typical runs were of about 5×10^6 steps, one step consisting of n particles moves.

We studied first the case of clusters in the neighborhood of $n = 10$ particles which is expected to be sufficient to observe the micellization process due to the single layer clustering¹⁰.

To this aim we started with an initial configuration of two pentagons with particles at their vertices juxtaposed one above the other. The two pentagons are parallel to the $x - y$ plane, have the z axis passing from their centers, and are one at $z = +\sigma/2$ and the other at $z = -\sigma/2$. The unit vectors attached to the spheres were chosen so to connect the origin to the center of the given sphere. We obtained the clusters with a lower number of particles by simply deleting particles and obtained the clusters with a higher number of particles by adding on the z axis a particle just above the upper pentagon and/or just below the lower one. However the results of the simulations are independent of the initial configuration chosen.

In order to compare with previous studies⁹, we consider the $\Delta = 0.5\sigma$ case first.

We performed the simulations of the isolated cluster and we have explicitly tested that results coincide with the calculation stemming for the bulk low density Janus fluid from which we extract cluster informations by taking all the cluster found with the same size and averaging their properties.

During the simulation we allow all possible moves but we do not count the configurations which are not topologically connected, i.e. those configurations where it is not possible to go from one sphere to all the others through a path; the path being allowed or not to move from one particle 1 to particle 2 depending whether $\Phi(12)$ has value $-\epsilon$ or not.

At high temperatures the limiting value for the energy per particle is $-\epsilon(n-1)/n$. At low temperature ($k_B T/\sigma < 0.15$) the clusters tend to freeze into certain energy minima. This can be improved by “regularizing” the angular part of the Kern-Frenkel potential into

$$\Psi(\hat{\mathbf{n}}_1, \hat{\mathbf{n}}_2, \hat{\mathbf{r}}_{12}) = \{\tanh[l(\hat{\mathbf{n}}_1 \cdot \hat{\mathbf{r}}_{12} - \cos\theta_0)] + 1\} \{\tanh[l(-\hat{\mathbf{n}}_2 \cdot \hat{\mathbf{r}}_{12} - \cos\theta_0)] + 1\} / 4. \quad (5.1)$$

and gradually increase l starting from $1/2$ during the simulation up to values where there is no actual difference between the continuous potential and the original stepwise one. This allowed us to reach the configuration with the real minimum energy with a certain confidence.

In Fig.1 we depict the relative cluster population N_n/N as a function of the reduced density $\rho\sigma^3$ in the ideal-gas case for $n \leq 12$ and two different temperatures $k_B T/\epsilon = 0.25$ (top panel) and $k_B T/\epsilon = 0.30$ (bottom panel). Temperature values were selected to bracket the expected critical temperature $k_B T/\epsilon \approx 0.28$ on transition from a vapor phase mostly formed by monomers (at higher temperatures) and a vapor phase with predominant clusters (at lower temperatures) in the chosen range of densities.¹⁰

As expected, we observe a predominance of monomers and higher order clusters at low and high density respectively. No significant difference is apparent for the results of the two temperatures. This is most likely due to the ideal-gas nature of the interacting part and can be improved by using the Carnahan-Starling fluid description, as we shall see.

Next we consider the internal energy per particle $u_n = \langle U \rangle/n$ within the n -th cluster along with the gyration radii defined by

$$R_g^2 = \sum_{j=1}^n |\mathbf{r}_j - \mathbf{r}_{av}|^2 / n \quad (5.2)$$

with $\mathbf{r}_{av} = \sum_{j=1}^n \mathbf{r}_j/n$, \mathbf{r}_j being the position of the j -th particle. Results for both internal energy and gyration radii for such configurations are tabulated in Table I. This provides an additional insight on the morphologies of the obtained clusters, in particular on the relative weak n dependence of the linear size of the obtained clusters.

The results for u_n as a function of temperature are reported in Table II and can be conveniently fitted by a Gaussian profile

$$u_n(T) = a_n \exp[-b_n T^2] + c_n, \quad (5.3)$$

where the fitting parameters a_n, b_n , and c_n for the $n = 2, 3, \dots, 12$ clusters ($u_1 = 0$ by definition) can also be found in Table II.

From this expression we can determine the excess free energy of the cluster $f_n^{\text{ex, intra}} = \beta F^{\text{ex, intra}}/n$ by thermodynamic integration

$$f_n^{\text{ex, intra}}(\beta) = \int_0^\beta dx u_n(1/x) \quad (5.4)$$

So that $f_n^{\text{intra}} = f_n^{\text{ex, intra}} + f_n^{\text{id, intra}}$ with the ideal free energy contribution being

$$f_n^{\text{id, intra}}(\beta) = 3 \ln \Lambda_n + (\ln n!)/n - \ln v_0, \quad (5.5)$$

where $v_0 = \pi\sigma_0^3/6$ is the volume of one n -cluster and $\Lambda_n = \sqrt{2\pi\beta\hbar^2/m_n}$ is the de Broglie thermal wavelength, and with the excess part given by

$$f_n^{\text{ex, intra}} = c_n\beta + a_n\sqrt{b_n} \left\{ \frac{e^{-b_n/\beta^2}}{\sqrt{b_n/\beta^2}} + \sqrt{\pi} \left[\text{erf}\left(\sqrt{b_n/\beta^2}\right) - 1 \right] \right\}. \quad (5.6)$$

The intra-cluster partition function is then $Z_n^{\text{intra}} = v_0^n e^{-n f_n^{\text{ex, intra}}}$ (of course $Z_1^{\text{intra}} = v_0$), where $v_0 = (\pi/6)\sigma_0^3$ is the volume of one cluster. As anticipated we here choose $\sigma_n = \sigma_0$, for all n , where σ_0 is the only undetermined parameter in the theory.

VI. ADDITIONAL RESULTS

A. Carnahan-Starling results

In this case the theory depends upon the average diameter of a cluster σ_0 . This is obtained by the requirement that the Carnahan-Starling results best match MC results for the bulk simulations.

To this aim, we consider Monte Carlo results at $\rho\sigma^3 = 0.01$ on the vapor phase, for the distribution of the cluster sizes, with our theory. This is depicted in Fig. 2 where we compare the Carnahan-Starling approximation with the MC data for the distribution of cluster sizes at decreasing values of temperatures starting from $k_B T/\epsilon = 0.5$ which provides a good match with MC results for $\sigma_0 \approx 2.64\sigma$. This value is then used in all subsequent calculations.

It is important to remark that, in order to find the correct solution for this system of equations, it is important to choose the one that is continuously obtained from the solution of the ideal gas case at $\sigma_0 \rightarrow 0$.

At lower temperatures the discrepancy with the MC data for the vapor increases. This was to be expected in view of the fact that the two-layer vesicles (n -clusters with $n = 40$) contribution to the vapor phase, and not included in the present computation, becomes increasingly important¹⁰. The agreement could be clearly improved by allowing a temperature dependence of the effective cluster diameter σ_0 , but we have chosen to keep σ_0 fixed to maintain a clear control of the approximations involved in our approach.

In Fig. 3 (top panel) we show the resulting cluster distribution for the N_n/N as a function of density for a temperature ($k_B T/\epsilon = 0.27$) at the onset of the expected critical micelle concentration¹⁰. Unlike previous case with ideal gas, there is now a clear predominance of the $n \approx 10$ clusters in the whole concentration range. Additional insights can be obtained by plotting the monomer density $\rho_1\sigma^3$ versus the total concentration $\rho\sigma^3$ for decreasing temperatures, as reported in the bottom panels of the same Figure, where the result of the present approach is contrasted with bulk numerical simulations of the same quantity¹⁰. This clearly shows the onset of a critical concentration where clusterization becomes the predominant mechanism at each temperature (this can be obtained by extrapolating the flat part of the curves to the vertical axis).

In order to assess the range of reliability of our results, we have also attempted to include in the theory all clusters of size up to 20 particles. Fig. 4 shows how the theory compares with the MC results at $k_B T/\epsilon = 0.4$ for the distribution

of the cluster sizes. Note that the vertical axis spans about 8 order of magnitudes. Here we used a slightly different value $\sigma_0 \approx 2.92\sigma$ for the cluster diameters. Our theory nicely follows the MC data for the vapor phase up to $n \leq 12$. For larger clusters discrepancies begin to show up most likely due to the fact isolated clusters tend to frequently disaggregate during the simulation thus providing a very low acceptance ratio. As anticipated, for this larger cluster sizes, a full simulation of the bulk vapor phase begins to be competitive with the present methodology, and this is the main reason why, in the remaining of the paper, we only consider a mixture of n -clusters with $n \leq 12$.

As remarked, the present theory depends upon a free parameter (the average cluster diameter σ_0) that is computed by a best fit with the bulk MC simulations.

Fig. 5 displays the sensitivity of some of the computed quantities to the choice of the average cluster diameter σ_0/σ . In particular, we have considered the compressibility factor $\beta P/\rho$, the internal energy per particle $u = U/N$ and the reduced free energy per particle $\ln(Q_{\text{tot}})/N$. In all cases, there is a non-negligible dependence on the σ_0/σ value indicating the importance of selecting the correct effective cluster diameter. This could be improved by considering a distribution of cluster diameters.

Notice that as σ_0 increases the packing fraction of the clusters η_t quickly exceeds unit, thus limiting the possible range of acceptance for the cluster diameter. Similarly, in Fig. 6 we report the compressibility factor and the excess internal energy per particle. The excess internal energy is compared with the MC data for the vapor phase⁹.

B. Prediction for a different range of the square well

So far, we have considered the case where the range of interaction (the width of the square well) Δ was 50% of the particle size σ . This is the value which has been exploited in details in past MC studies of the bulk Janus fluid^{9,10}. As this range decreases, typical relevant temperatures decrease and simulations become increasingly more demanding from the computational point of view to equilibrate. It is then no surprising that no results have been yet reported in the literature for these ranges. On the other hand, these are the ranges most frequently encountered in the experiments²⁶, and this is where the usefulness of our method can be assessed.

We have then repeated the calculations for $\Delta/\sigma = 0.25$, that is half of previous value.

Fig. 7 reports the cluster distributions for the ideal and the Carnahan-Starling fluids (lower temperatures), and are the counterpart of Figs. 1 and 3. Concentrations of the n -clusters are now shifted towards higher densities with respect to the case with the twice as wide range, as expected. Also now the role of the 10-cluster and the 11-cluster is inverted respect to before. This means that lower attractive range provides, on average, smaller stable clusters, a results that can be understood on intuitive basis.

We also found that thermodynamic quantities considered above are only marginally affected by the reduction of the width well in the considered range of densities and temperature.

We have also considered the case of $\Delta = 0.15\sigma$. From Fig. 8 it is apparent that the concentrations of the n -clusters are once again shifted towards higher densities respect to the case with $\Delta = 0.25\sigma$. Also now the 7- and 8-clusters seems to be the ones favoured at $T = 0.27$ in a range of densities in a neighborhood of $\rho\sigma^3 = 0.1$. This confirms the trend found in the case $\Delta = 0.25\sigma$.

VII. CONCLUSIONS

In this paper, we have constructed a cluster theory for the vapor of Janus fluid. This is an approach that is complementary to previous studies based on highly demanding MC simulations^{9,10}, with the aim of providing a detailed description of the vapor phase in view of its remarkable unusual micellization properties.

The main idea behind the present approach is to consider the vapor phase as formed by clusters, containing an increasing number of particles, that are weakly interacting among each other so that simple fluid models – such as ideal gas or hard spheres – can be used to mimic their physical properties. The internal degrees of freedom of each clusters are instead obtained through a direct MC simulation of a single isolated cluster, a much simpler task as compared to the bulk simulation and a procedure akin to those used in the framework of simple fluids¹⁶ is then used to combine the two calculations and obtain the full description of the system.

It is worth noticing that, in the ideal-gas case, a similar procedure has also been already implemented in micellization theories by several groups^{27,28}, and the results we obtain in the present context are quite consistent with those.

There are two basic reasons why we expect this approach to be valuable. First because previous full bulk simulations showed micelles to be only weakly interacting in the vapor density range and hence a simple description for the inter-cluster part is expected to be sufficient. Second, because it has been observed that the vapor properties are mostly dominated by particular cluster sizes corresponding to $n \approx 10$ and $n \approx 40$ particles, so only a limited number of cluster sizes is necessary to obtain a complete description.

In the present work, we have considered clusters up to 12 particle and compared the ideal-gas description with the description of a gas of hard-sphere spheres, mimicking the original clusters and with an effective cluster diameter σ_0 , using the Carnahan-Starling approximate description. The value of σ_0 has been obtained by a matching of the results for the internal energy with full bulk MC simulations. A good agreement was found at $k_B T/\epsilon = 0.5$ and at densities $\rho\sigma^3 = 0.01$ when $\sigma_0 \approx 2.64\sigma$. Results from Carnahan-Starling theory is found to be far superior as compared to the ideal-gas description, thus emphasizing the importance of inter cluster correlations in the vapor phase.

We also considered higher sizes clusters (of up to 20 particles) but the agreement with the simulations for the larger sizes becomes less satisfactory. The theory becomes less and less accurate as oscillations in the behavior of the concentrations of the big clusters with size appear. This may be due to the difficulty in an accurate determination of the internal energy of isolated big clusters. On this respect in order to be able to observe the vesicles (clusters of around 40 particles⁹) phenomenology we certainly need to include additional insights to avoid the task of the solution of a system of about 40 coupled equations. An additional difficulty consists in the fact that in this case the single diameter effective approximation used for all clusters up to 12 in the present study, will no longer be realistic, not even at the simplest possible level of description. Both these problems could be tackled by focussing only on clusters bracketing the interesting ones ($n \approx 10$ and $n \approx 40$ in the present case).

We showed that in accord with the simulation results of Ref. 9, at temperatures around $k_B T/\epsilon = 0.27$ there is a gap of densities where the number of clusters of 11 particles (micelles) surpasses the number of any other cluster. This gap shrinks as we increase the temperature.

The determined approximation to the partition function of the vapor phase of the Janus fluid can then be used to compute various thermodynamical quantities.

We found reasonable quantitative agreement between the Monte Carlo data of Ref. 9 and our theory for the excess internal energy of the vapor phase of the Janus fluid. We additionally computed the compressibility factor for which no simulation data are yet available.

Having validated the model against numerical predictions for $\Delta = 0.5\sigma$ we pursued the analysis for lower widths of the well, values that are closer to the experimental range of interactions²⁶. In view of the overall decrease in the attractions, characteristic critical temperatures also decrease, thus making numerical simulations increasingly demanding from the computational point of view.

For the case $\Delta = 0.25\sigma$ we produced new predictions for the concentrations, the compressibility factor, and the internal energy per particle as a function of density. In particular we saw that as the range of the attraction diminishes the Janus fluid prefer to form cluster of a lower number of particles.

Consistent results are also found for the case $\Delta = 0.15\sigma$, a value which rather close to those used in experiments.

An attempt to push the cluster theory to bigger cluster sizes showed that the theory becomes less and less accurate as oscillations in the behavior of the concentrations of the big clusters with size appear. This may be due to the difficulty in an accurate determination of the internal energy of isolated big clusters. On this respect in order to be able to observe the vesicles (clusters of around 40 particles⁹) phenomenology we certainly need to include additional insights to avoid the task of the solution of a system of about 40 coupled equations. An additional difficulty consists in the fact that in this case the single diameter effective approximation used for all clusters up to 12 in the present study, will no longer be realistic, not even at the simplest possible level of description. Both these problems could be tackled by focussing only on clusters bracketing the interesting ones ($n \approx 10$ and $n \approx 40$ in the present case).

Two additional perspectives will be the subject of a future study. First the dependence on coverage χ could also be tackled using the present approach, and this would provide invaluable information on the micellization mechanism for small coverage, a task that is still out of reach to direct numerical simulations. Secondly, it would be extremely interesting to address the issue of the reentrant phase diagram and the (possible) existence of an additional liquid-liquid critical point. This has been recently attempted in a very recent preprint²⁹, using a monomer-cluster equilibrium theory in the same spirit of that presented here.

Acknowledgments

RF would like to acknowledge the support of the National Institute of Theoretical Physics of South Africa. AG acknowledges the support of a PRIN-COFIN 2007B58EAB grant. FS acknowledges support from ERC-226207-PATCHYCOLLOIDS and ITN-234810-COMPLOIDS.

* Electronic address: rfantoni27@sun.ac.za

† Electronic address: achille@unive.it

- [‡] Electronic address: francesco.sciortino@phys.uniroma1.it
- [§] Electronic address: pastore@ts.infn.it
- ¹ V. N. Manoharan, M. T. Elsesser, and D. J. Pine, *Science* **301**, 483 (2003)
- ² A. B. Pawar and I. Kretzchmar, *Macromol. Rapid Commun*, **31**, 150 (2010)
- ³ S. C. Glotzer and M. J. Solomon, *Nature Materials* **6**, 557 (2007)
- ⁴ Z. Zhang and S. C. Glotzer, *Nano Letters* **4**, 1407 (2004)
- ⁵ P. G. de Gennes, *Rev. Mod. Phys* **64**, 645 (1992)
- ⁶ C. Casagrande, P. Fabre, M. Veyssié, and E. Raphaël, *Europhys. Lett* **9**, 251 (1989)
- ⁷ L. Hong, A. Cacciuto, E. Luijten, and S. Granick, *Nano Letters* **6**, 2510 (2006)
- ⁸ A. Walther and A. H. Müller, *Soft Matter* **4**, 663 (2008)
- ⁹ F. Sciortino, A. Giacometti, and G. Pastore, *Phys. Rev. Lett.* **103**, 237801 (2009)
- ¹⁰ F. Sciortino, A. Giacometti, and G. Pastore, *Phys. Chem. Chem. Phys.* **12**, 11869 (2010)
- ¹¹ N. Kern and D. Frenkel, *J. Chem. Phys.* **118**, 9882 (2003)
- ¹² M. S. Wertheim, *J. Stat. Phys.* **35**, 19 (1984); *J. Stat. Phys.* **35**, 35 (1984); *J. Stat. Phys.* **42**, 459 (1986), *J. Stat. Phys.* **42**, 477 (1986)
- ¹³ G. T. Evans, *J. Chem. Phys.* **106**, 9718 (1997)
- ¹⁴ M. E. Fisher and D. M. Zuckerman, **109**, 7961 (1998)
- ¹⁵ J. Dudowicz, J. F. Douglas, and K. F. Freed, *J. Phys. Chem. B* **112**, 16193 (2008)
- ¹⁶ A. Tani and D. Henderson, *J. Chem. Phys.* **79** 2390 (1983)
- ¹⁷ N. Bjerrum, *Kgl. Danske Vidensk. Seiskab* **7**, 9 (1926)
- ¹⁸ J. L. Barrat and J. P. Hansen, *Basic Concepts for Simple and Complex Liquids*, (Cambridge University Press 2003)
- ¹⁹ F. Sciortino, E. Bianchi, J. F. Douglas, and P. Tartaglia, *J. Chem. Phys.* **126**, 194903 (2007)
- ²⁰ T. Boublík, *J. Chem. Phys.* **53**, 1523 (1970)
- ²¹ G. A. Mansoori, N. F. Carnahan, K. E. Starling, and T. W. Leland Jr., *J. Chem. Phys.* **54**, 1523 (1971)
- ²² N. F. Carnahan and K. E. Starling, *J. Chem. Phys.* **51**, 635 (1969)
- ²³ J. P. Hansen and I. R. McDonald *Theory of Simple Liquids* 2nd Ed. (Academic Press 1986)
- ²⁴ M. P. Allen and D. J. Tildesley *Computer Simulation of Liquids* (Oxford Univ. Press 1987)
- ²⁵ N. Metropolis, A. W. Rosenbluth, M. N. Rosenbluth, A. H. Teller, and E. Teller, *J. Chem. Phys.* **21**, 1087 (1953)
- ²⁶ L. Hong, A. Cacciuto, E. Luijten, and S. Granick, *Langmuir* **24**, 621 (2008)
- ²⁷ R. Nagarajan and E. Ruckenstein, *Langmuir* **7**, 2934 (1991)
- ²⁸ J. N. Israelachvili, D. J. Mitchell and B. W. Ninham, *J. Chem. Soc. Faraday Trans.2* **72**, 1525 (1976)
- ²⁹ A. Reinhardt, A. J. Williamson, J. P. K. Doyle, J. Carrete, L. M. Varela and A. A. Louis, arXiv:1010.4676v1 cond-mat.soft (2010)

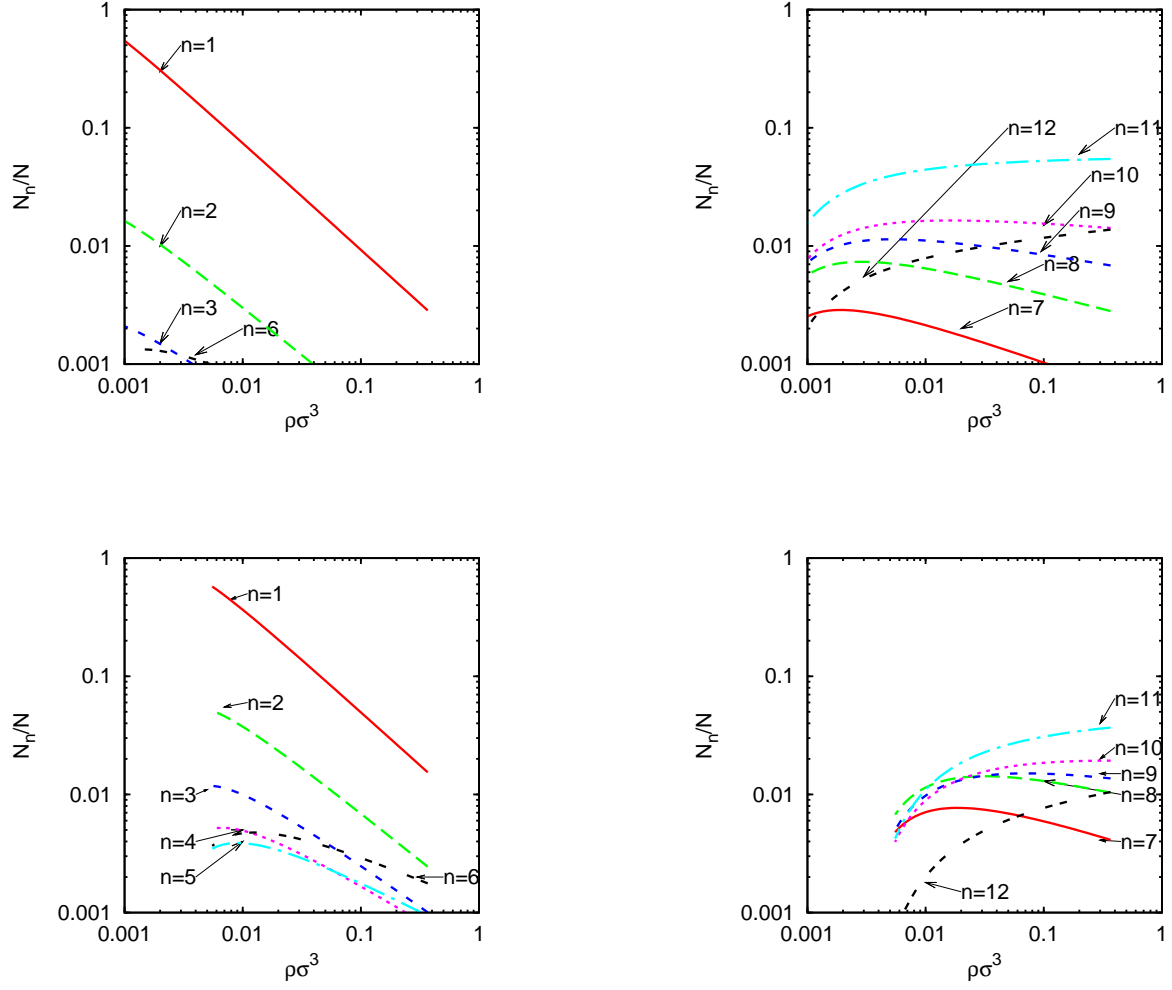


FIG. 1: Values of N_n/N , $n = 1, 2, 3, \dots, 12$ as a function of the density for $\Delta = 0.5\sigma$ and $k_B T/\epsilon = 0.25$ (top panels) and $k_B T/\epsilon = 0.30$ (bottom panels). In both cases curves for $n = 1, \dots, 6$ are on the left panels and those associated with $n = 7, \dots, 12$ are on the right panels. All plots have been reported on the same scale for a better comparison. Clusters associated with values $n = 4, 5$ have curves lying below the lower limit of 0.001 concentration in the case $k_B T/\epsilon = 0.25$.

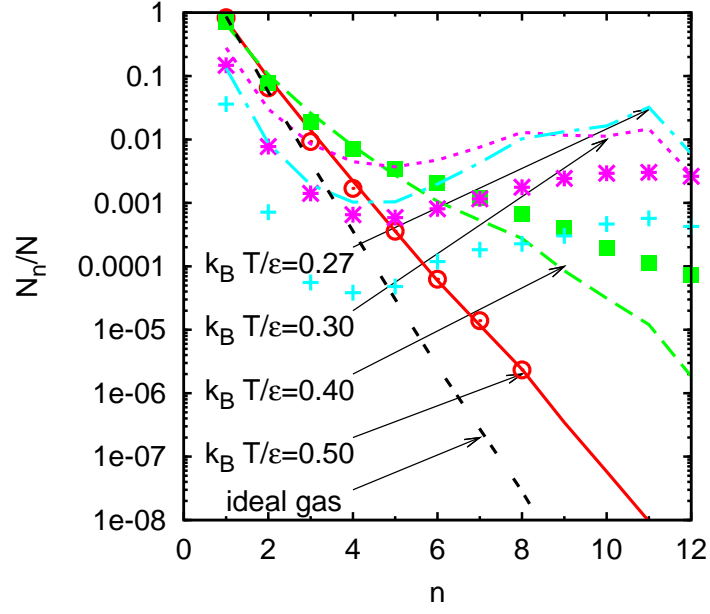


FIG. 2: Comparison between the MC data (points) and our calculations using the effective one component hard sphere inter-cluster partition function within Carnahan-Starling approximation for $\sigma_0 = 2.64\sigma$ (lines), for N_n/N , $n = 1, 2, 3, \dots, 12$ as a function of the clusters size n at $\rho\sigma^3 = 0.01$, $\Delta = 0.5\sigma$, and various temperatures. Also shown is the ideal gas approximation

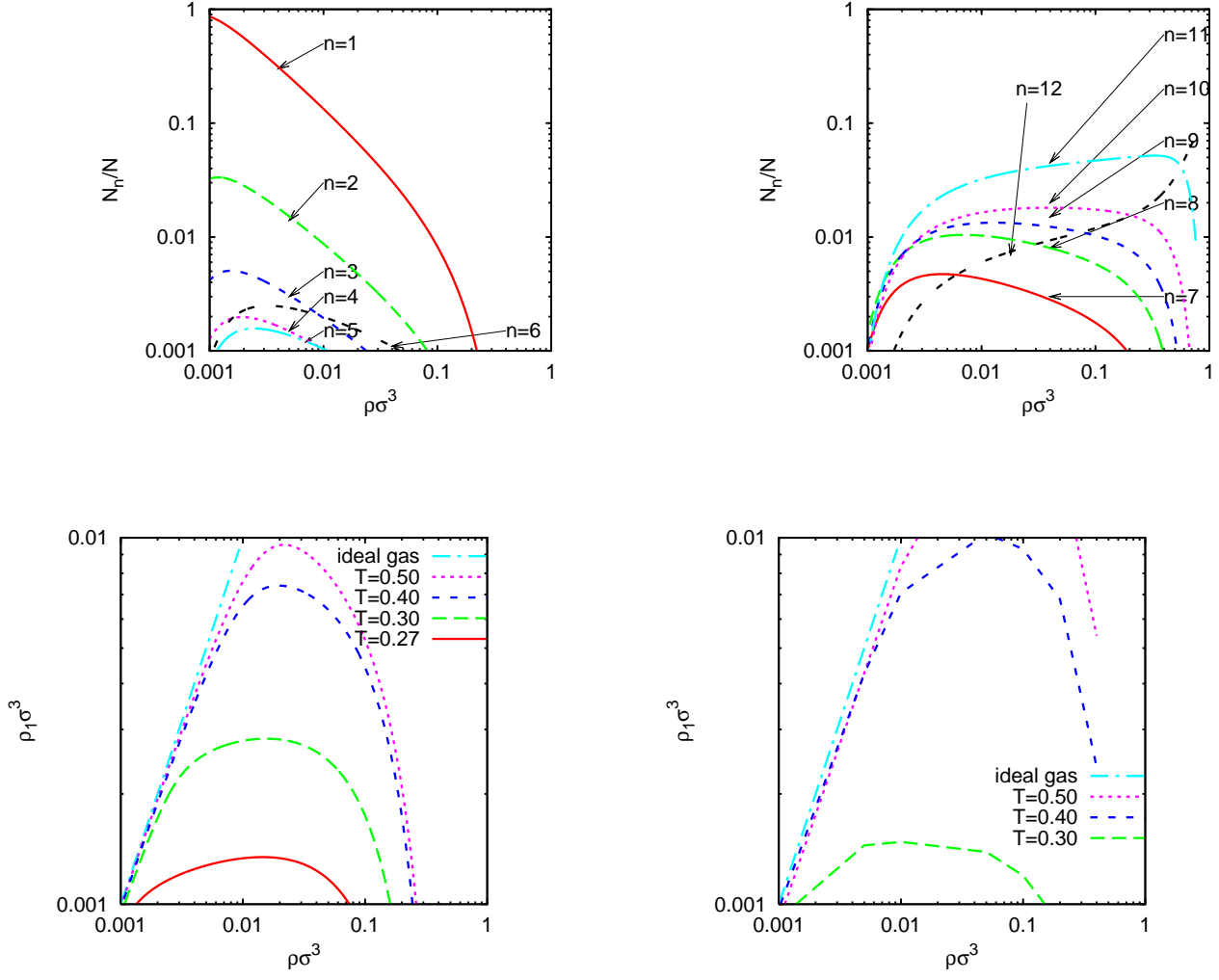


FIG. 3: Values of N_n/N , $n = 1, 2, 3, \dots, 12$ as a function of the density for $k_B T/\epsilon = 0.27$ (top panels). Clusters with $n = 1, \dots, 6$ are on the left, those with $n = 7, \dots, 12$ on the right. The bottom panels depict the monomer concentration $\rho_1\sigma^3$ as a function of the total density $\rho\sigma^3$ for decreasing temperatures. The result of the present approach (left) is contrasted with MC simulations (right). All results refer to the $\Delta = 0.5\sigma$ case with a cluster diameter $\sigma_0 = 2.64\sigma$.

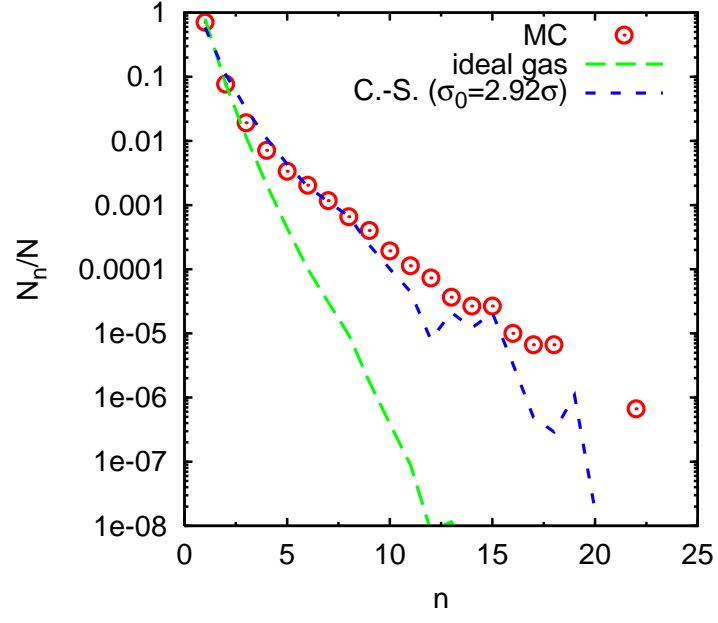


FIG. 4: Comparison between MC data and cluster theory using Carnahan-Starling approximation (for $\sigma_0/\sigma = 2.92$) for N_n/N , $n = 1, 2, 3, \dots, 20$ as a function of the clusters size n at $k_B T/\epsilon = 0.4$, $\rho\sigma^3 = 0.01$, and $\Delta = 0.5\sigma$.

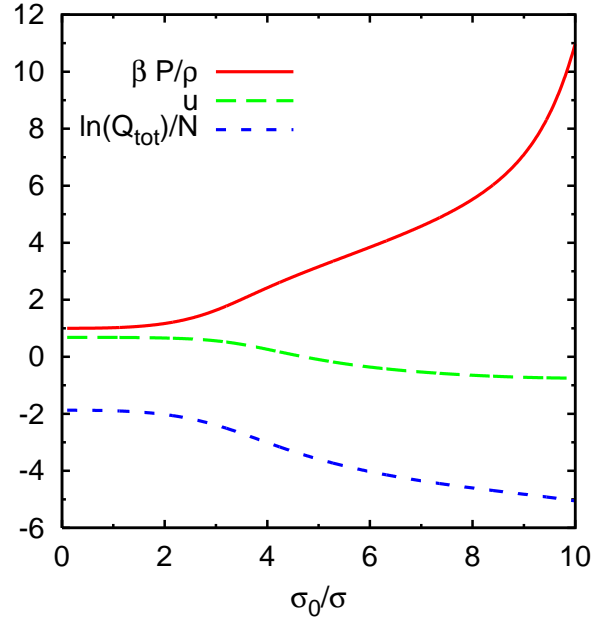


FIG. 5: Values for the compressibility factor, the internal energy per particle, and the logarithm of the total partition function as a function of the n -cluster diameter σ_0/σ at $\rho\sigma^3 = 0.01$, $k_B T/\epsilon = 0.5$, and $\Delta = 0.5\sigma$.

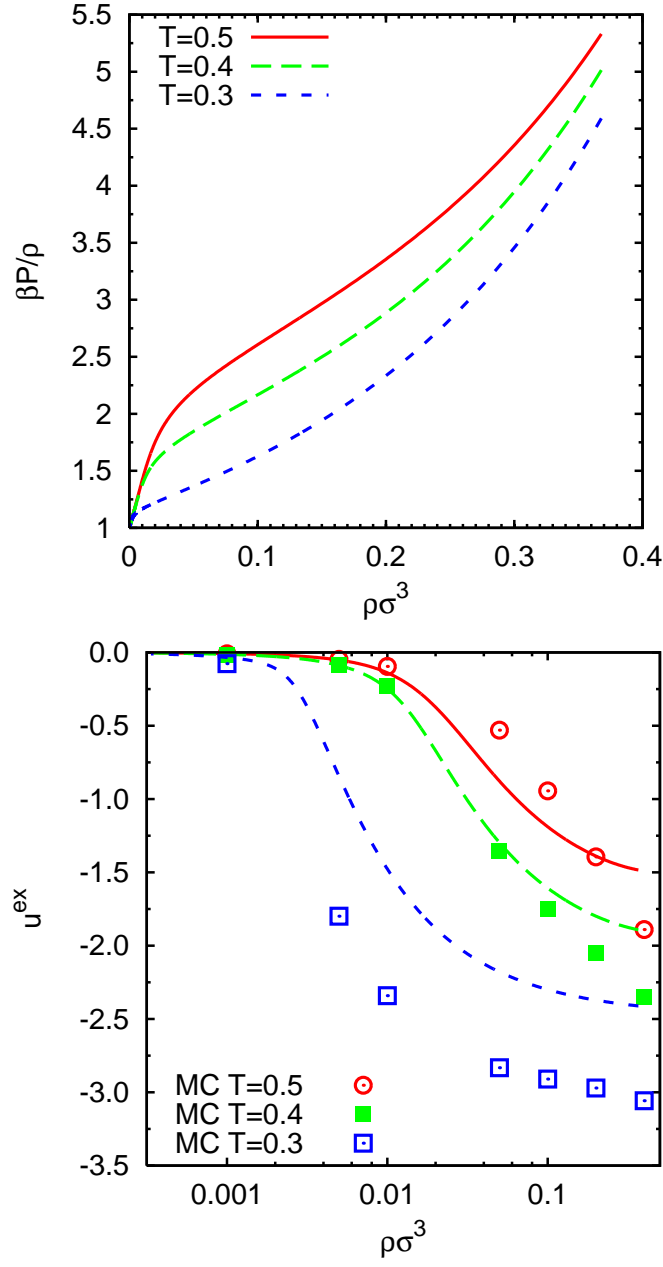


FIG. 6: Compressibility factor as predicted by the Carnahan-Starling ($\sigma_0 = 2.64\sigma$) cluster theory (top panel). On the bottom panel we compare the MC data and the Carnahan-Starling cluster theory (same diameter as above) for the excess internal energy per particle for three different values of temperatures. In all cases $\Delta = 0.5\sigma$.

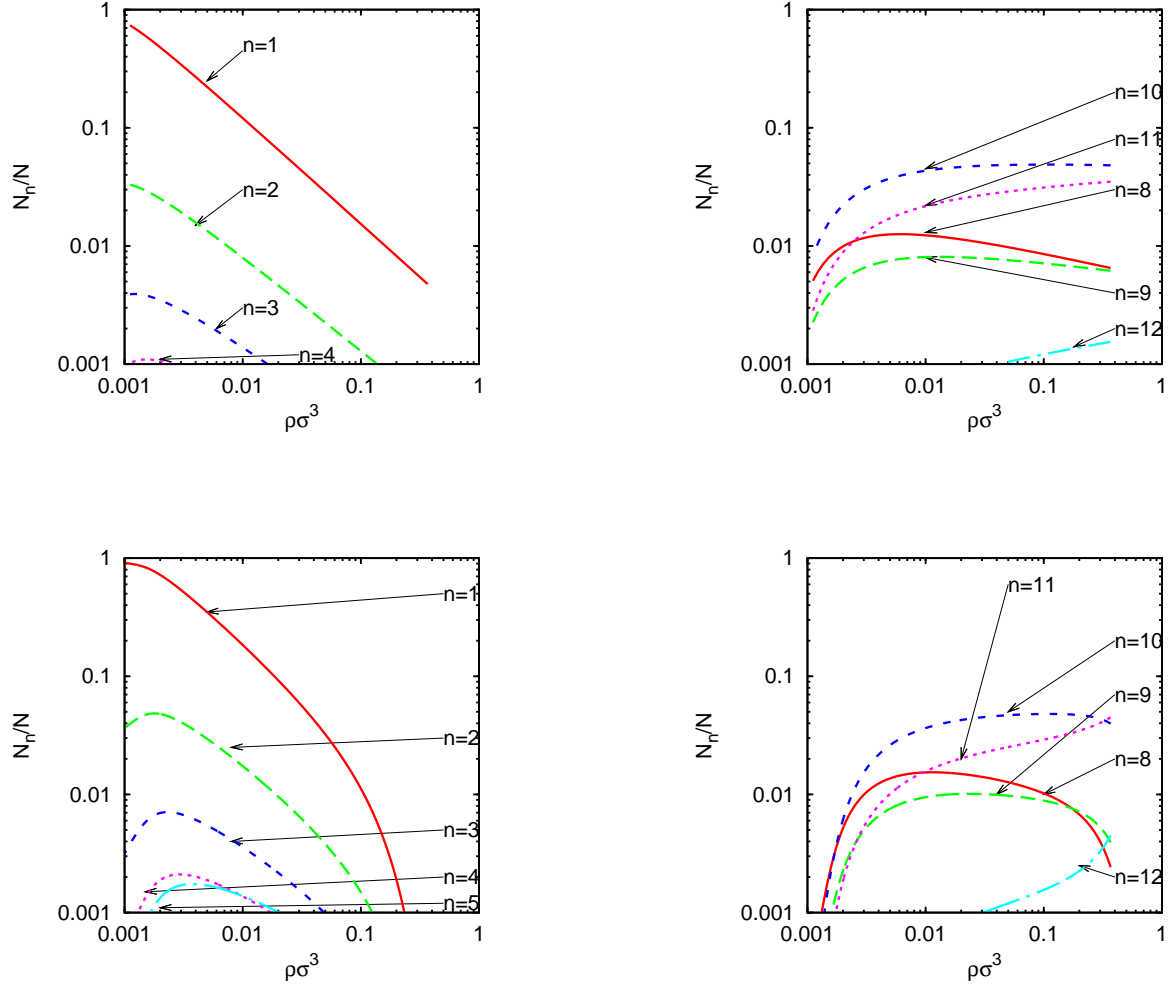


FIG. 7: Cluster distribution in the case $\Delta = 0.25\sigma$. The top panels report the ideal gas result at $k_B T/\epsilon = 0.25$ ($n = 1, \dots, 6$ on the left and $n = 7, \dots, 12$ on the right). This is the same as Fig. 1. The bottom panels depict with the same distribution of curves the results obtained with Carnahan-Starling approximation at $k_B T/\epsilon = 0.27$ which is the counterpart of Fig. 3

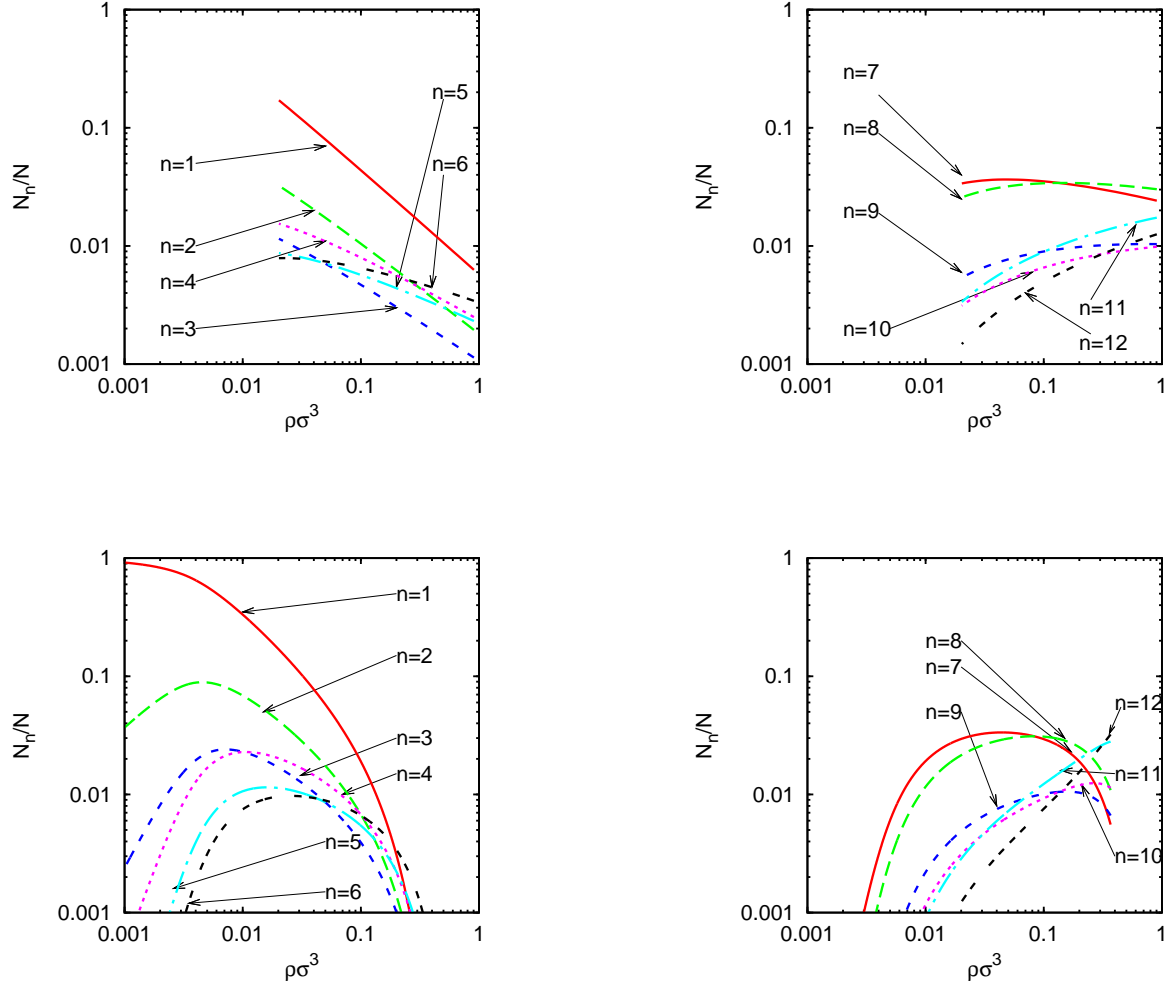


FIG. 8: Same as Fig. 7 for $\Delta = 0.15\sigma$.

n	$\langle U \rangle/n$	U	R_g
1	0	0	0
2	-0.5	-1	$\sim 1/2$
3	-1	-3	$\sim 1/\sqrt{3}$
4	-1.5	-6	0.83
5	-2.0	-10	0.76
6	-2.50	-15	0.75
7	-2.71	-19	0.91
8	-2.88	-23	0.93
9	-3.10	-28	0.96
10	-3.20	-32	1.00
11	-3.36	-37	1.04
12	-3.42	-41	1.08

TABLE I: The low temperatures internal energy per particle of the clusters with up to 12 particles when $\Delta = 0.5\sigma$. Also shown is the gyration radius R_g defined in Eq.(5.2) .

	$\Delta = 0.5\sigma$		$\Delta = 0.25\sigma$		$\Delta = 0.15\sigma$		
n	a_n	b_n	a_n	b_n	a_n	b_n	c_n
2	0	1	0	1	0	1	-0.50
3	-0.337	3.880	-0.339	6.905	-0.346	10.780	-0.67
4	-0.778	4.670	-0.771	7.502	-0.774	7.975	-0.75
5	-1.226	5.162	-1.025	5.890	-1.034	9.366	-0.80
6	-1.700	5.600	-1.381	7.361	-1.207	9.214	-0.83
7	-1.899	5.263	-1.423	6.767	-1.480	8.277	-0.86
8	-2.064	5.080	-1.520	4.179	-1.551	8.503	-0.88
9	-2.301	5.478	-1.579	4.367	-1.681	10.160	-0.89
10	-2.394	5.509	-1.725	4.271	-1.551	9.419	-0.90
11	-2.556	5.644	-1.846	4.829	-1.696	9.755	-0.91
12	-2.598	6.077	-1.854	5.723	-1.814	10.567	-0.92

TABLE II: Fit to a Gaussian of the energy per particle as a function of the temperature (see Eq. (5.3))
. c_n values are common to the three cases.